THE JOURNAL OF PHYSICAL CHEMISTRY B

Article

pubs.acs.org/JPCB

Dissecting Hydrophobic Hydration and Association

Richard C. Remsing*,† and John D. Weeks*,‡

†Institute for Physical Science and Technology and Chemical Physics Program, University of Maryland, College Park, Maryland 20742, United States

‡Institute for Physical Science and Technology, and Department of Chemistry and Biochemistry, University of Maryland, College Park, Maryland 20742, United States

ABSTRACT: We use appropriately defined short-ranged reference models of liquid water to clarify the different roles local hydrogen bonding, van der Waals attractions, and long-ranged electrostatic interactions play in the solvation and association of apolar solutes in water. While local hydrogen bonding interactions dominate hydrophobic effects involving small solutes, longer-ranged electrostatic and dispersion interactions are found to be increasingly important in the description of interfacial structure around large solutes. The hydrogen bond network sets the solute length scale at which a crossover in solvation behavior between these small and large length scale regimes is observed. Unbalanced long-ranged forces acting on interfacial water molecules are also important in hydrophobic association, illustrated here by analysis of the association of model methane and buckminsterfullerene solutes.

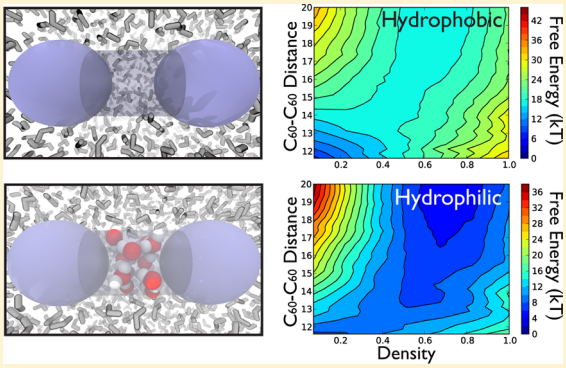

I. INTRODUCTION

Hydrophobic interactions play a key role in phenomena ranging from biological processes like protein folding and membrane formation to the design of water-repellent materials.[1−3] Thus, significant effort has been devoted to studying the behavior of apolar moieties in water. In pioneering work, Stillinger argued that hard sphere solutes smaller than a critical radius R_C can be inserted into liquid water while maintaining the hydrogen bond network, but for solutes with a radius larger than R_C bonds must be broken, generating a molecular scale interface with properties resembling that of the liquid−vapor interface in water.[4] More recent work has confirmed the basic features of this idea and put the arguments on a firmer statistical mechanical foundation.[2,3,5,6]

While this qualitative description of the length scale dependence of hydrophobic hydration seems physically very reasonable, it focuses only on the hydrogen bond network of water and makes no mention of the van der Waals (VDW) attractions and long-ranged multipolar interactions between water molecules or of the VDW attractions that would be present between a more realistic solute and the solvent. Moreover, a qualitatively similar length scale transition is seen in a dense Lennard-Jones (LJ) fluid near the triple point, with the formation of a "dry" vapor-like interface around a large hard sphere solute.[6] In that case, clearly there are no hydrogen bonds and the transition is generated solely by unbalanced VDW attractive forces arising from solvent molecules far from the solute.

Consideration of such unbalanced forces is an essential ingredient in the Lum−Chandler−Weeks (LCW) theory of hydrophobicity,[5] which uses the same basic framework to describe hard sphere solvation in simple liquids and in water, differing only in the thermodynamic parameters needed as input to the theory.[5,7,8] Indeed LCW theory has been criticized for not treating hydrogen bonds and other distinctive features of water more explicitly, and there has also been considerable debate about possible effects of solute−solvent LJ attractions on the proposed length scale transition in water.[3] Thus it seems useful to explore in more detail the varying roles hydrogen bonds, VDW interactions, and long-ranged multipolar interactions play in hydrophobic solvation, and to determine what analogies exist to solvation in simple, nonassociating fluids.

To that end, we build on our previous work[9] using truncated water models,[10] and exploit the underlying ideas of perturbation[11,12] and local molecular field[6,13] (LMF) theories of uniform and nonuniform fluids, respectively, to study hydrophobic solvation and association from small to large length scales. We employ short-ranged variants of the SPC/E water model to show that small-scale solvation and association in water is governed by the energetics of the hydrogen bond network alone. However, when the solute is large and the hydrogen bond network is broken at the hydrophobic interface, water behaves in a manner qualitatively similar to a simple fluid, with unbalanced LJ attractions dominating the solvation behavior.

Special Issue: Michael D. Fayer Festschrift

Received: May 29, 2013
Revised: July 26, 2013
Published: August 14, 2013

In the next section, the truncated water models are briefly introduced, and our simulation methods are detailed. Section III examines the roles of unbalanced dispersion and electrostatic forces in determining the equilibrium solvation structure around small and large apolar solutes. The strength of the hydrogen bond network around small solutes is then analyzed by perturbing the hydration shell in Section IV. The role of this network in setting the length-scale for the crossover in solvation thermodynamics is then studied in Section V. The origin of entropy convergence is briefly discussed in Section VI. Finally, the hydrophobic association of model methane and fullerene molecules is studied in Section VII. Our conclusions and a discussion of the implications of this work are given in Section VIII.

II. MODELS AND SIMULATION DETAILS

Hydrogen bonds in most classical water models arise from "frustrated charge pairing", where an effective positive charge on a hydrogen site of one molecule tries to get close to a negatively charged acceptor site on a neighboring molecule.[9] This strong attractive interaction is opposed by the overlap of the repulsive LJ cores and the presence of other hydrogen sites in the acceptor molecule. As a result, short-ranged versions of the full water model where Coulomb interactions are truncated at distances larger than the hydrogen bond length and with only truncated LJ core interactions if desired can still give a very accurate description of the hydrogen bond network and pair correlation functions in bulk water.[9,15]

In this work, we use the extended simple point charge (SPC/E) model of water[14] and two previously developed short-ranged variants of this model[9] to examine hydrophobic hydration and association as the solute perturbs the hydrogen bond network. The truncated models provide a hierarchical framework for disentangling in such classical models the separate contributions of (i) strong short-ranged interactions leading to the hydrogen bond network, (ii) longer-ranged VDW attractions between water molecules and with the solute, and (iii) long-ranged dipolar interactions between water molecules.

The first such model, the *Gaussian-truncated* (GT) water model, has full LJ interactions but truncated Coulomb interactions.[9,15] It thus lacks the long-ranged electrostatics necessary to provide a description of the physical multipolar interactions that act over large distances. We also utilize the *Gaussian-truncated repulsive-core* (GTRC) model,[9] where both the long-ranged electrostatic interactions and the long-ranged LJ attractions have been removed. The GTRC model generates a minimal reference network model that captures very well the structure of the local hydrogen bond network in bulk water while ignoring effects of the remaining long-ranged Coulomb and dispersion interactions.

In order to compare the SPC/E water model at a pressure of $P = 1$ atm with the short-ranged GT and GTRC models in the work presented below, the latter two models were simulated at corrected pressures yielding the same density using the pressure corrections described previously.[9,16] There it was shown that simple analytical corrections to the pressure can bring the bulk densities of these three models into quantitative agreement. All data presented in this work were obtained from molecular dynamics simulations performed in the isothermal−isobaric ensemble (constant NPT) using a modified version of the DL_POLY2.18 software package.[17] Constant temperature and pressure conditions were maintained through the use of a Berendsen thermostat and barostat, respectively.[18] The evaluation of electrostatic interactions in simulations of the full SPC/E water model employed the Ewald summation method.[19]

It is instructive to compare the solvation behavior of water to that of a simple LJ fluid at an analogous state point throughout this work. Therefore, following the work of Huang and Chandler,[7] we also study an LJ fluid at a state point near the triple point, where the potential is truncated and shifted at 2.5σ. This LJ fluid is studied at a reduced temperature and pressure of $T^* = k_BT/\varepsilon = 0.85$ and $P^* = P\sigma^3/\varepsilon = 0.022$, respectively, corresponding to a reduced density of $\rho^* = \rho\sigma^3 = 0.70$. In order to study the analogous short-ranged reference fluid, we use the same repulsive force truncation of the LJ potential as was used for the GTRC water model, and study the model at a mean-field corrected pressure that accounts for the lack of LJ attractions.[9]

We should emphasize that the above-mentioned short-ranged GT and GTRC models are *not* being used in this paper as replacements for standard long-ranged models such as SPC/E or to give accurate representations of most properties of real water. Rather, we utilize these models as *analysis tools* to examine the different roles the hydrogen bond network as described by the GT or GTRC models, long-ranged dispersions, and dipolar interactions play in determining the properties of systems containing liquid water. For this purpose, the failings of the short-ranged models are just as instructive as their successes.

However, the GT model describes very well pair correlation functions and hydrogen bond statistics in bulk water, and as we discuss further below, it also captures many features of the water density in nonuniform environments including the basic length scale transition for hydrophobic solutes.[9] However, thermodynamic and particularly electrostatic properties depend sensitively on the long-ranged Coulomb interactions, and GT results need corrections for quantitative accuracy. Acharya and Garde[20] have recently carried out a detailed study of the strengths and weaknesses of the GT model as a simple water model in a variety of settings, including both hydrophobic and ionic solvation.

III. THE INFLUENCE OF LONG-RANGED INTERACTIONS ON INTERFACIAL STRUCTURE

In this section, we examine the role of the various unbalanced forces in determining the interfacial structure of water near a hydrophobic solute. The solute is considered to be a uniform density of LJ particles, such that its interaction with water can be represented by an integration of the LJ potential over the volume of the solute, resulting in the integrated "9−3" potential of Huang and Chandler[21]

$$U_{SW}(r; R_S) = \pi\varepsilon_{sw}\rho\sigma_{SW}^3 \times \left[\frac{4}{5}\sigma_{SW}^9\left(\frac{1}{8rr_+^8} - \frac{1}{9r_+^9} - \frac{1}{8rr_-^8} + \frac{1}{9r_-^9}\right) - 2\sigma_{SW}^3\left(\frac{1}{2rr_+^2} - \frac{1}{3r_+^3} - \frac{1}{2rr_-^2} + \frac{1}{3r_-^3}\right)\right] \quad (1)$$

where $r_\pm = r \pm R_S$. The parameters of the potential are chosen to mimic paraffin, such that the density of LJ sites, energy, and length scale are given by $\rho = 0.0240$ Å^{-3}, $\varepsilon_{sw} = 0.882$ kJ/mol, and $\sigma_{sw} = 3.468$ Å, respectively.[21] Furthermore, in order to make this particle as hydrophobic as possible, only the repulsive

dx.doi.org/10.1021/jp4053067 | J. Phys. Chem. B 2013, 117, 15479−15491

part of the potential is used, such that the solute-water interaction potential used in the MD simulations is given by

$$U_{0,sw}(r) = \begin{cases} U_{sw}(r) - U_{sw}(r_0), & r \le r_0 \\ 0, & r > r_0 \end{cases} \quad (2)$$

where r_0 is the location of the minimum of the potential. Finally, we should note that the size of the particles is better represented through an effective hard-sphere radius, R_{HS}, rather than the size parameter R_S found in the potential. This effective radius can be estimated as[22]

$$R_{HS} \approx \int_0^\infty dr\{1 - \exp[-\beta U_{0,sw}(r)]\} \quad (3)$$

where $\beta = (k_B T)^{-1}$, and will be reported as R_{HS} herein.

The hydration structure around small solutes has been postulated to be a direct consequence of the need for water to maintain its hydrogen bond network. A small solute can be "inserted" into bulk water with the network continuing around the solute without breaking hydrogen bonds. Indeed, in the small solute regime we find that the nonuniform densities of GT and GTRC models around an apolar particle are nearly identical to that of the full SPC/E water, dramatically confirming that local hydrogen bonding dictates the hydration structure in this limit (Figure 1a).

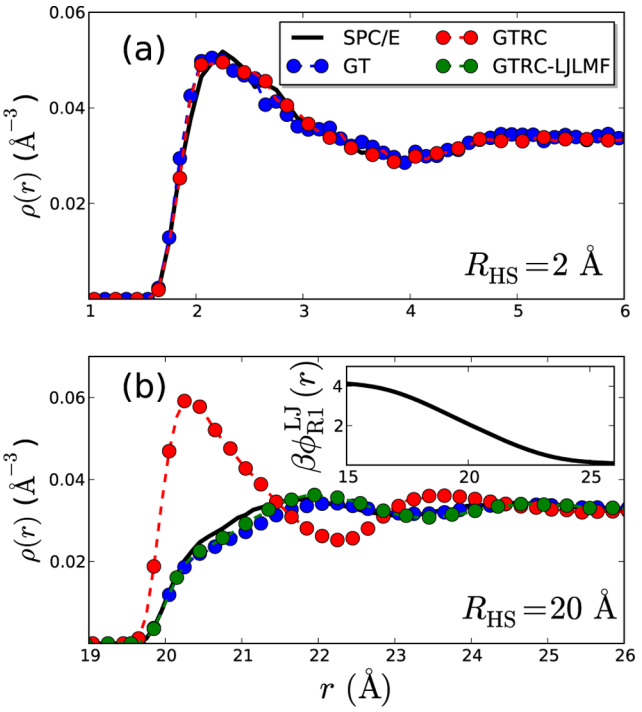

Figure 1. Density distributions around solutes of radii $R_{HS} \approx 2$ Å (a) and $R_{HS} \approx 20$ Å (b). The inset in (b) depicts the renormalized portion of the LJ LMF for GTRC water in units of $k_B T$.

In the large solute limit, Figure 1b, the density profiles of SPC/E and GT water are still very similar, demonstrating that long-ranged electrostatic interactions have an almost negligible influence on this measure of interfacial structure. GTRC water, on the other hand, has a $\rho(r)$ markedly different from that of SPC/E water.

Removal of the LJ attractions from the bulk liquid in GTRC water eliminates the phenomena of drying, and it evidentially wets the surface of the solute. According to LMF theory,[13] we can account for the averaged effects of the neglected LJ forces by using a renormalized solute field

$$\phi_R^{LJ}(\mathbf{r}) = U_{0,sw}(r) + \int d\mathbf{r}'[\rho_R(\mathbf{r}') - \rho_B]u_1(|\mathbf{r} - \mathbf{r}'|) \quad (4)$$

where quantities obtained in the presence of the effective field are indicated by the subscript "R" throughout this work, ρ_B is the bulk density of the fluid, and $u_1(r)$ is the attractive portion of the LJ potential. The use of this renormalized field recovers drying behavior and brings the density profile of GTRC water into qualitative agreement with that of the SPC/E and GT models, as illustrated by the curve labeled "GTRC-LJLMF" in Figure 1b. The renormalized portion of the LMF, $\phi_{R1}^{LJ}(\mathbf{r}) \equiv \phi_R^{LJ}(\mathbf{r}) - U_{0,sw}(r)$, provides an effective force that pushes solvent molecules away from the solute, as shown in the inset of Figure 1b.

From the data presented in Figure 1, we can conclude that the unbalanced forces arising from LJ attractions are the driving force for drying at extended hydrophobic interfaces. Indeed, we have previously shown that the net force on a water molecule at an extended hydrophobic interface from long-ranged electrostatics is much smaller than that from LJ attractions.[9] Nevertheless, long-ranged electrostatics play a subtle but important role in determining the orientational preferences of water and properties dependent upon this orientational structure. One such quantity is the electrostatic or polarization potential $\Phi(r)$ felt by a test charge

$$\Phi(r) = -\int_0^r dr' \mathcal{E}(r') = -\int_0^r \frac{dr'}{r'^2} \int_0^{r'} dr'' r''^2 \rho^q(r'') \quad (5)$$

where $\rho^q(\mathbf{r}) \equiv \langle \Sigma_i q_i \delta(\mathbf{r} - \mathbf{r}_i) \rangle$ is the ensemble averaged charge density of the system and $\mathcal{E}(r)$ is the electric field due to the polarization of water molecules induced by the presence of the solute.

The polarization potential of SPC/E water, shown in Figure 2a, reaches a constant value of approximately 500 mV in the bulk region, consistent with previous determinations of interface potentials at extended hydrophobic interfaces for this water model.[15] Removal of the long-ranged electrostatic interactions in GT water leads to an approximate charge density that does not predict this plateau in the bulk region (Figure 2a). Thus there is a net electric field $\varepsilon(r)$ in this system, even far from the solute surface as shown in Figure 2b. The appearance of a nonvanishing electric field in the bulk of GT water is associated with an overorientation of interfacial OH bonds toward the solute surface. This is evidenced by a larger peak at $\theta_{OH} \approx 0°$ in the probability distribution $P(\theta_{OH})$ for interfacial GT water molecules in comparison to that observed for SPC/E water, shown in Figure 2c, where θ_{OH} is the angle formed by the OH bond vector and the oxygen-solute vector

The increase in the number of OH groups pointing toward the interface in GT water is driven by the tendency to maintain the hydrogen bond network alone. This results in the formation of an overly ordered dipole layer at the interface, demonstrated by the peak at $\theta_\mu \approx 60°$ in $P(\theta_\mu)$, shown in Figure 2d, where θ_μ is the angle formed by the dipole vector of water and the oxygen-solute vector. Without long-ranged dipole−dipole interactions, water far from the surface does not respond to the presence of this dipole layer, and $\mathcal{E}(r)$ remains nonzero

dx.doi.org/10.1021/jp4053067 | J. Phys. Chem. B 2013, 117, 15479−15491

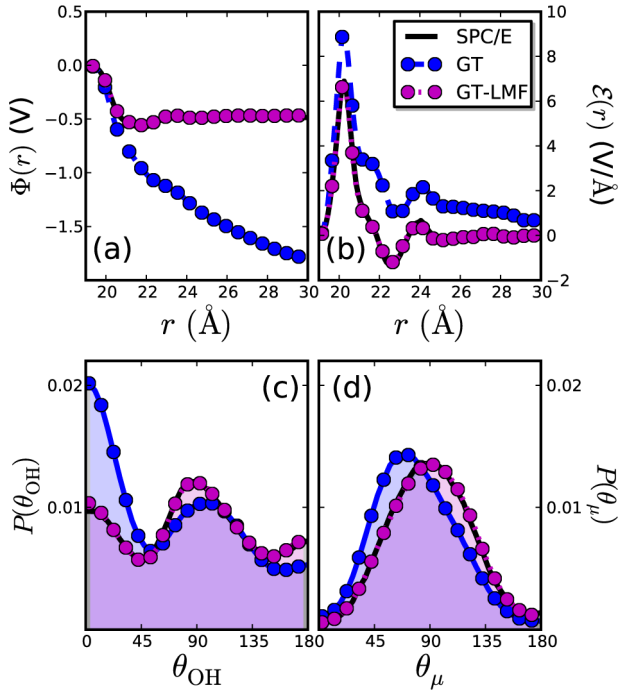

Figure 2. (a) Polarization potential $\Phi(r)$ and (b) the corresponding electric fields $\mathcal{E}(r)$ obtained for a solute of $R_{HS} \approx 20$ Å in SPC/E and GT water, as well as for GT water in the presence of the electrostatic LMF (GT-LMF). (c) Probability distributions of the angle formed by the OH bond vector and the vector connecting the oxygen site with the center of the solute (θ_{OH}), for molecules within 1 Å of the solute surface for the three systems shown in (a). The analogous distributions for the dipolar angle θ_μ are shown in (d).

well into the bulk region. However, we can compensate for the averaged effects of the long-ranged electrostatics through the introduction of the electrostatic LMF for an uncharged solute[13]

$$\mathcal{V}_R(\mathbf{r}) = \int d\mathbf{r}' \rho_R^q(\mathbf{r}') v_1(|\mathbf{r} - \mathbf{r}'|) \tag{6}$$

where $v_1(r) = \mathrm{erf}(r/\sigma)/r$ is the long-ranged, slowly varying component of $1/r$, separated with a smoothing length $\sigma = 4.5$ Å[9] herein, and in general σ should be chosen to be greater than the nearest-neighbor distance in a fluid.[13] Inclusion of this renormalized solute potential in the GT water system leads to quantitative accuracy of both the electrostatic and orientational structure of interfacial water, evidenced by the curves labeled GT-LMF in Figure 2.

In his seminal work on nonpolar solutes in aqueous solutions, Stillinger deduced that orienting an OH bond toward the interface provides the least energetic detriment to the hydrogen bond network of water.[4] In GT water, there are no opposing long-ranged electrostatic interactions, and the energetics of the hydrogen bond network alone determines the orientational preferences of water at the interface. However, this results in too high a probability of pointing an OH bond toward the interface, illustrating that while hydrogen bonding is a major driving force in determining the structure of water around large apolar solutes, it is not the sole determinant of the observed orientational preferences of interfacial water.

In an earlier contribution, Stillinger and Ben-Naim initially postulated that the dipole and quadrupole moments of water lead to a mean torque on a molecule at the interface with its vapor that orients the dipole moment of an interfacial water molecule toward the bulk liquid.[23] This behavior is reflected in the change of $P(\theta_\mu)$ upon the inclusion of long-ranged interactions through $\mathcal{V}_R$, which provides the slowly varying torque necessary to slightly turn the molecular dipoles of interfacial water in the direction of the bulk and obtain the desired orientational structure, evidenced by the distributions $P(\theta_\mu)$ shown in Figure 2d. Therefore, the orientational structure of water at extended hydrophobic surfaces is a result of a delicate balance of the energetics of the hydrogen bond network *and* the mutipolar interactions arising from the electrical asymmetry of a water molecule, with the former dominating.

IV. THE RESPONSE OF INTERFACIAL WATER TO UNBALANCED FORCES

In this section, we examine the response of short-ranged reference systems around solutes of varying sizes to the presence of very strong unbalanced forces like those seen in reality only for very large solutes. This provides a stringent test of the stability of the hydrogen bond network around small solutes even when subjected to strong perturbations. In order to accomplish this task, we scale the long-ranged LJ LMF determined for a large solute of radius $R_{HS} \approx 20$ Å by its radius, and then rescale the field to the desired solute size, $\tilde{R}_{HS}$,

$$\tilde{\phi}_{R1}(r;\, \lambda,\, \tilde{R}_{HS}) = \lambda \phi_{R1}^{LJ}\left(\frac{\tilde{R}_{HS}}{R_{HS}} r;\, R_{HS}\right) \tag{7}$$

where $\phi_{R1}^{LJ}(\mathbf{r})$ is the slowly varying renormalized portion of the LMF shown in the inset of Figure 1b. Here the notation $\phi_{R1}^{LJ}(r;R_{HS})$ indicates that the field ϕ_{R1}^{LJ} is a function of r and that it was determined when a solute of radius R_{HS} is fixed at the origin. The fictitious, rescaled LMF is indicated by $\tilde{\phi}_{R1}$, and the coupling parameter λ is used to further adjust the magnitude of this field. In effect we have taken the large unbalanced LJ force around a large solute, which Figure 1b shows is strong enough to significantly perturb the large-scale density profile of GTRC water when corrected with LMF theory, and artificially applied it to a small scale system like that in Figure 1a with an intact local hydrogen bond network. This provides insight into the very different response interfaces around small and large hydrophobic solutes have to repulsive forces over a wide range of magnitude as λ is varied, including exceptionally large unbalanced forces seen in reality only near large hydrophobic solutes.

In order to quantify the response of water to strong unbalanced forces, we focus on the λ-dependence of the average number of water molecules in the solute solvation shell, $\langle N(\lambda)\rangle_{\tilde{\phi}_{R1}}$, as well as the corresponding response function

$$\chi(\lambda) = -\frac{1}{\langle N(0)\rangle_{\tilde{\phi}_{R1}}}\left(\frac{\partial \langle N(\lambda)\rangle_{\tilde{\phi}_{R1}}}{\partial \lambda}\right) \tag{8}$$

where $\langle ... \rangle_{\tilde{\phi}_{R1}}$ indicates that the ensemble average is performed in the presence of the field $\tilde{\phi}_{R1}(r;\lambda,\tilde{R}_{HS})$. The function $\langle N(\lambda)\rangle_{\tilde{\phi}_{R1}}$ is calculated for distances $r < r_{min}$, where r_{min} is defined as the distance at which the density distribution in the absence of the field reaches its first minimum.

In the large scale hydration regime, the broken hydrogen bonds in the interfacial region effectively permit the interface to detatch from the solute, and the interface is "soft" and fluctuating. We expect water to have a response qualitatively

dx.doi.org/10.1021/jp4053067 | J. Phys. Chem. B 2013, 117, 15479−15491

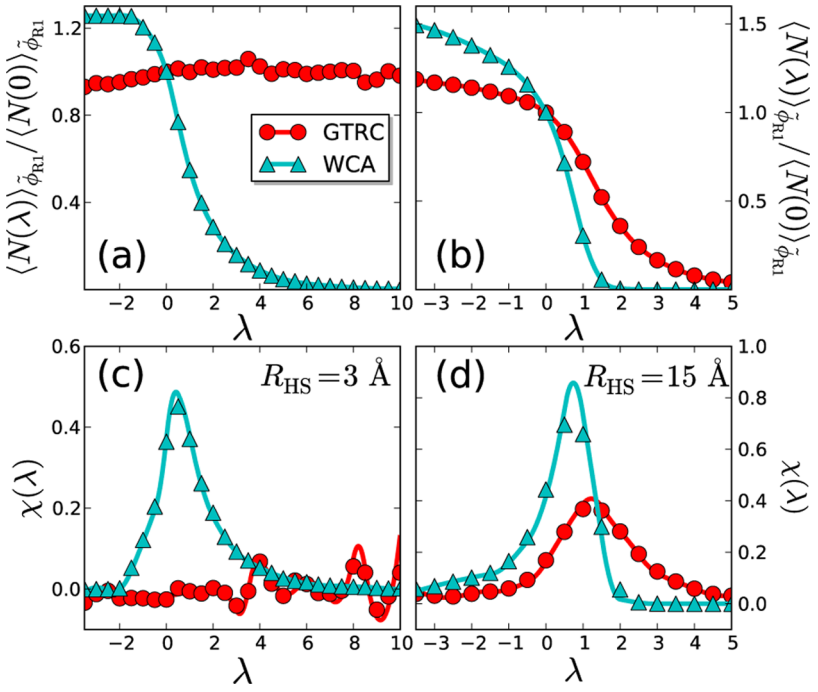

Figure 3. Average number of truncated water and LJ molecules in the first solvation shell as a function of the coupling parameter λ for solutes of radii $R_{HS} \approx 3$ Å (a) and $R_{HS} \approx 15$ Å (b). Results are shown for both GTRC water and the WCA fluid (with the LJ parameters of SPC/E water), and $\langle N(\lambda)\rangle_{\tilde{\phi}_{R1}}$ has been normalized by its value in the case of zero field in order to make comparisons between the two fluids. The corresponding response functions are shown in (c) and (d), respectively. Solid lines in (a) and (b) are spline fits to $\langle N(\lambda)\rangle_{\tilde{\phi}_{R1}}$ and those in (c) and (d) are the negative derivatives of the corresponding fits.

similar to that of simple liquids where drying occurs with increasing strength of $\tilde{\phi}_{R1}$. However, in the small length scale limit, while network fluctuations certainly occur, the hydrogen bond network is basically maintained around the solute. We thus expect that the small scale solute-water interface is "stiff" and highly resistant to perturbations unless they are strong enough to break hydrogen bonds. This should lead to behavior that is fundamentally different from that of a simple LJ fluid, which lacks such strong, local interactions.

As postulated above, in the large solute regime, the behavior of $\langle N(\lambda)\rangle_{\tilde{\phi}_{R1}}$ and $\chi(\lambda)$ are qualitatively similar for both GTRC water and the WCA fluid (Figure 3b and Figure 3d). Gradual dewetting is observed with increasing field strength, until no molecules are present in the solvation shell region at high values of the coupling parameter. In fact, as λ is increased, a peak in the response function χ is observed, indicative of a drying transition in the hydration shell of the solute; the details of the transition differ between GTRC water and the WCA fluid due to differences in state points and interaction potentials.

In the small solute regime, the WCA fluid displays signatures of a drying transition completely analogous to those seen in the large solute case with a simple shift in λ. GTRC water, on the other hand, does not display characteristics of such nanoscale dewetting (Figure 3a,c); $\langle N(\lambda)\rangle_{\tilde{\phi}_{R1}}$ stays roughly constant, and the response function fluctuates about zero. Using a typical geometric definition of a hydrogen bond,[9,24] we find that the average number of hydrogen bonds per molecule, for waters located between the solute and the position of the first maximum in the corresponding $\rho(r)$, fluctuates around 3.5 for all $\lambda \geq 0$, very close to the bulk value of 3.6 hydrogen bonds per water molecule. Therefore, the hydrogen bond network is maintained around the small solute for all studied values of λ, and the strong local interactions of the hydrogen bond network prohibit drying at the solute surface, even in the presence of the extremely large external fields considered herein.

The above-described results indicate that the underlying physics behind the solvation behavior in a LJ fluid is qualitatively similar in the small and large length scale regimes, dependent only on the magnitude of the unbalancing potential arising from the bulk, while that of water qualitatively differs in the two regimes. In the large length scale regime, water behaves in a manner similar to an LJ fluid, with the unbalanced LJ attractions having a substantial impact on the solvation structure. For solutes smaller than the crossover radius, however, water wets the surface of the solute even in the presence of extremely large (though fictitious) unbalancing potentials; the hydration shell remains intact due to the great strength of the local hydrogen bond network. Therefore, interfacial fluctuations and the physics dictating where the length scale transition occurs is different for water than for simple, non-hydrogen bonding fluids.

V. HYDROGEN BONDING SETS THE SCALE FOR THE CROSSOVER IN HYDRATION THERMODYNAMICS

The above-described physical balance between hydrogen bonding and interfacial unbalancing potentials also plays a key role in the solvation thermodynamics of apolar solutes. Gibbs free energies of solvation, ΔG, were calculated by performing equilibrium simulations of solutes with effective hard sphere radii $R_{HS} \leq 13$ Å in increments of $\Delta R_{HS} \approx 0.5$ Å. Due to poor phase space overlap between neighboring windows, ΔR_{HS} was decreased to 0.25 Å to determine ΔG for solutes with $R_{HS} > 7$ Å solvated by GTRC water. The

dx.doi.org/10.1021/jp4053067 | J. Phys. Chem. B 2013, 117, 15479−15491

solvation free energies presented herein were calculated using the Bennett acceptance ratio or BAR[25,26] method. To emphasize the crossover in the scaling behavior of the solvation free energies, we normalize ΔG by the surface area of the apolar solute (Figure 4), $\Delta\tilde{G} = \Delta G/4\pi R_{HS}^2$.

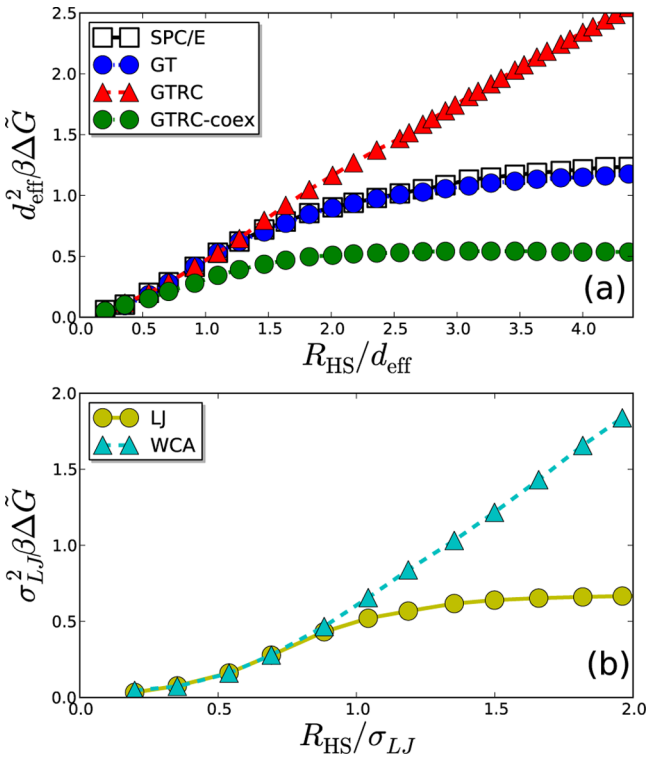

Figure 4. Solvation free energies of apolar spheres per unit solute area as a function of solute radius, scaled by the effective diameter of a corresponding solvent molecule (d_{eff} = 2.75 Å for water), for (a) SPC/E, GT, and GTRC water models, as well as (b) a LJ fluid and its corresponding WCA reference system. Error bars are smaller than the symbols shown.

In the small solute regime, $R_{HS} \leq R_C \approx 5.0$ Å, the hydration free energies are in agreement for all three models. This illustrates that the hydration thermodynamics of small, nonpolar solutes are dictated by the local structure of water alone, as would be expected from the conclusions drawn above regarding solvation in the SPC/E, GT, and GTRC models. Indeed, the dominant role of local structure in the small solute regime is not restricted to water, as indicated by the agreement of the solvation free energies for LJ and WCA fluids for small solute sizes shown in Figure 4b.

The free energy for large solutes scales with surface area in both SPC/E water and the LJ fluid, and here long-ranged interactions become increasingly important. Only small differences in ΔG are observed between SPC/E and GT water, reflecting the relatively small role of long-ranged electrostatics in hydrophobic hydration.[9] LJ attractions, on the other hand, make a substantial contribution to the hydration free energy. Indeed because of the absence of these attractions, GTRC water completely lacks the plateau in $\Delta\tilde{G}$ for large solute sizes.

The behavior of the GTRC water model can be explained by noting that in the large solute regime, $\Delta G \sim PV_S + \gamma A_S$, where V_S and A_S are the volume and surface area of the solute, respectively, P is the pressure of the system, and γ is the solute-water surface tension. In order to obtain the same bulk density as SPC/E water at a pressure of 1 atm, the GTRC model must be maintained at a pressure of roughly 3 katm. At this state, the GTRC water model is far from liquid−vapor coexistence, and the pressure is large enough to make the PV_S term dominate the behavior of ΔG for large solutes.

However, we have previously shown that GTRC water can indeed have a self-maintained liquid−vapor interface, but at a lower bulk density close to that of ice. The interface is maintained by the strong short-ranged Coulomb attractive forces between donor and acceptor sites and the need to preserve as many hydrogen bonds as possible.[9] However, because there are no unbalanced forces from LJ attractions, the surface tension is much smaller than that of the full SPC/E model.

As shown in the curve labeled "GTRC-coex" in Figure 4a, the solvation free energies in GTRC water near coexistence in both the small and large solute regimes are smaller in magnitude than those in SPC/E water. However, it exhibits essentially the same crossover radius as the full SPC/E model and scales with solute surface area for large solutes. The behavior of ΔG below the crossover radius can be understood from our previous results for the bulk structure of the GTRC model near coexistence.[9] The bulk coexistence density is close to that of ice, and the hydrogen bond network has a more ordered tetrahedral structure that can more readily accommodate the formation of a cavity than is the case for SPC/E water.

Although the solvation free energies of apolar solutes in water and in the LJ fluid exhibit qualitatively similar crossover behavior, they differ in one important respect: the length scale at which the crossover in solvation behavior occurs. For the LJ fluid, the crossover radius is approximately equal to the diameter of a solvent particle. At this solute size, the unbalanced forces from the LJ attractions of the bulk region become large enough to "pull" particles away from the solute surface, leading to drying.

Although unbalanced LJ forces also exist when apolar particles of similar size are solvated by water, the possible disruption of strong local hydrogen bonds between interfacial water molecules dominates the energetics, and the crossover occurs only when water is not able to maintain this network. This leads to an estimate for the crossover radius, $R_C \approx 5$ Å, almost twice the diameter of a water molecule (2.75 Å) and significantly larger than that found in a LJ fluid. As shown above, hydrophobic solvation in GTRC water near coexistence also displays a crossover in its scaling behavior at a value of R_C essentially the same as that of the full SPC/E model. Because GTRC water accounts only for the hydrogen bond network, we can conclusively say that the crossover in solvation behavior is determined by the hydrogen bond network of water alone, occurring when the solute size is increased to a point beyond which it is impossible for this network to remain intact, consistent with the original arguments of Stillinger.[4]

Given the importance of the hydrogen bond network for small scale solvation in water, how can we rationalize the success of the LCW theory[5] and related lattice models incorporating similar physics,[35,36] which lack an explicit description of hydrogen bonds? These theories correctly describe the small scale physics driven by Gaussian density fluctuations in the bulk solvent and the large scale physics dominated by the formation of a vapor-like interface around a large repulsive solute. Effective parameters controlling the transition between the two regimes are fit to experimental data for each particular solvent.

dx.doi.org/10.1021/jp4053067 | J. Phys. Chem. B 2013, 117, 15479−15491

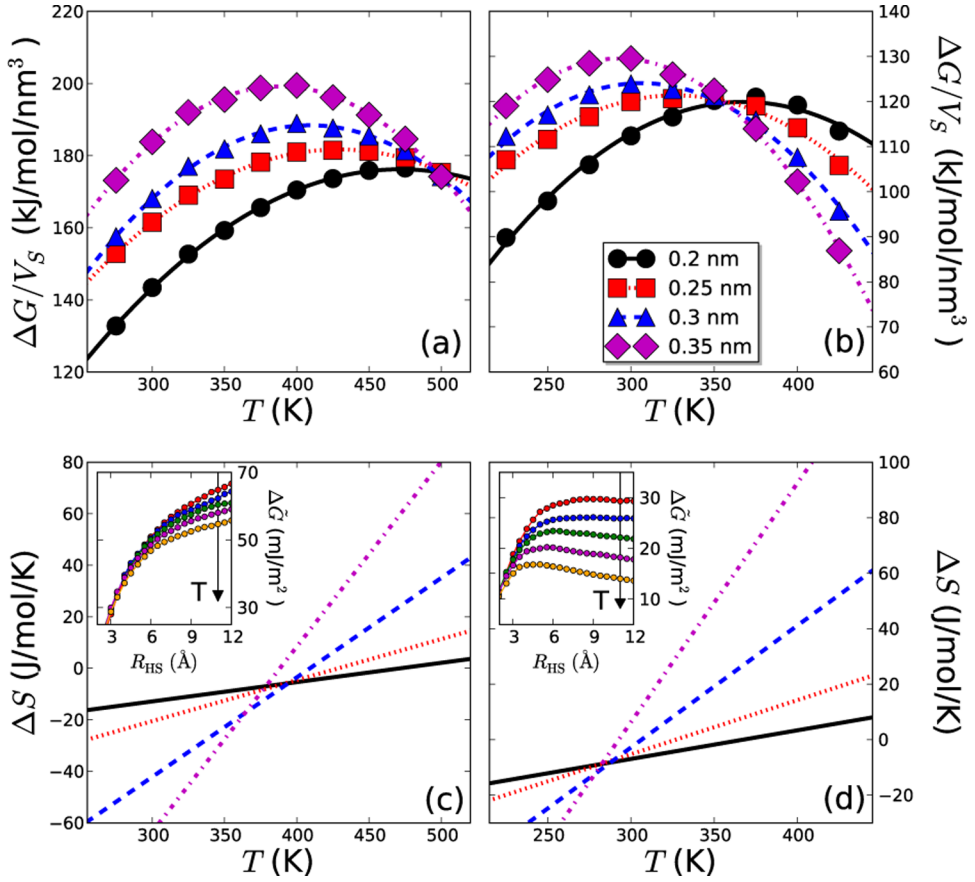

Figure 5. Hard sphere solvation free energy ΔG per unit solute volume V_S as a function of temperature in (a) SPC/E and (b) GTRC water. The corresponding entropies of solvation ΔS as a function of T are shown in (c) and (d), respectively. Hard sphere radii are indicated in the legend. Solvation free energies as a function of solute size for T = 300 K, 325 K, 350 K, 375 K, and 400 K are shown in the insets of (c) and (d) for the SPC/E and GTRC models, respectively. The arrows point in the direction of increasing temperature.

The key experimental parameters determining the transition length scale in the LCW theory are the liquid−vapor surface tension, and the bulk density and compressibility. The small compressibility and large surface tension of water compared to an LJ fluid implicitly accounts for the strength of the hydrogen bond network in bulk water and the difficulty of disrupting it by interface formation for large solutes. This allows the LCW theory to qualitatively describe the different transition length scales in both water and an LJ fluid[7] using the same basic framework. However, LCW theory uses mean field ideas and square gradient and other approximations, and errors are seen in its detailed predictions for certain other properties like the interface width.[7] More detailed approaches describing structure and fluctuations in both small and large length scale regimes are needed for quantitative calculations.

More recent work by Rajamani, Truskett, and Garde[38] has clarified the relation between bulk thermodynamics and the crossover radius. They suggested that the crossover radius is proportional to the Egelstaff−Widom length scale $l_{EW} = \gamma\kappa_T$, the product of the liquid−vapor surface tension γ, and the isothermal compressibility κ_T.[37] Quantitative agreement can be achieved by using a microscopic compressibility that depends on the solute volume rather than the long wavelength bulk compressibility in conjunction with the solute−water interfacial tension to estimate the crossover radius R_C.

A simple but stringent test of this idea is to compare the Egelstaff−Widom length scale of GTRC water near liquid−vapor coexistence to that of SPC/E water. As discussed above, the crossover radius in GTRC water is essentially the same as in SPC/E water. This is easily rationalized from our microscopic understanding of the very similar behavior of the hydrogen bond network around the solute in GTRC and SPC/E water. If this simple physics is reflected in the Egelstaff−Widom length scale, this too should be nearly the same, although both the surface tension and bulk compressibility differ considerably in the two models.

Indeed, the compressibility κ_T^{GTRC} of GTRC water at T = 300 K and a pressure of 1 atm is 0.087 katm^{-1}, roughly a factor of 2 larger than that of SPC/E at the same state point, 0.045 katm^{-1}, while the surface tension of the GTRC model γ^{GTRC} ≈27 mN/m, is about half of that of the SPC/E model $\gamma^{SPC/E}$ ≈54.7 mN/m. Here the value for SPC/E water was taken from the work of Sedlmeier and Netz,[39] and the surface tension of GTRC water was estimated by extrapolating the solvation free energies $\Delta\tilde{G}(R_{HS})$ presented in Section V to the limit $R_{HS}\to\infty$. Thus, the Egelstaff−Widom length scales of SPC/E and GTRC water are nearly equal, $l_{EW}^{SPC/E}$ = 0.24 Å and l_{EW}^{GTRC} = 0.23 Å, respectively, as expected.

VI. ENTROPY CONVERGENCE IS A CONSEQUENCE OF THE HYDROGEN BOND NETWORK

The temperature dependence of hydrophobic hydration also displays features distinct from solvation in typical VDW liquids. Specifically, hydration free energies ΔG of small apolar particles increase with increasing temperature along a significant portion

dx.doi.org/10.1021/jp4053067 | J. Phys. Chem. B 2013, 117, 15479−15491

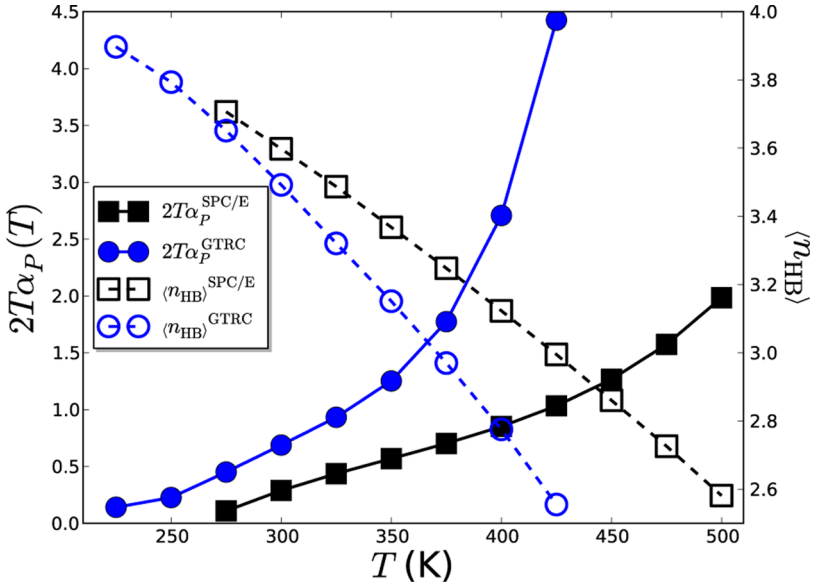

Figure 6. Thermal expansion coefficient multiplied by twice the temperature (left axis, closed symbols) and average number of hydrogen bonds per water molecule (right axis, open symbols) for SPC/E and GTRC water.

of the coexistence curve until a maximum is reached. Above this temperature, free energies of solvation decrease with increasing temperature, a behavior typical of most fluids. Associated with this region of anomalous solvation is the phenomenon of *entropy convergence*, in which the hydration entropies, $\Delta S = -(\partial \Delta G/\partial T)_P$, intersect near a temperature of 400 K for a large range of solute sizes, although the location of the hydration free energy maximum varies somewhat with solute size. Analogous to the discussion of the crossover length scale, the explanation of entropy convergence typically uses thermodynamic arguments, citing the small and nearly constant compressibility of water along the liquid−vapor coexistence line, relative to organic solvents,[40−42] although explanations exist that do not hinge on the relative incompressibility of bulk water.[43]

In this section, we show that entropy convergence in water arises from the hydrogen bond network through its impact on bulk thermodynamics by studying the temperature dependence of hard sphere solvation in the SPC/E and GTRC water models near liquid−vapor coexistence. Simulations of bulk SPC/E and GTRC water were carried out at a pressure of 1 atm and temperatures ranging from 275 to 500K and 225 to 425K, respectively. Hard sphere solvation free energies in the small solute regime were determined by assuming Gaussian bulk density fluctuations,[40,41,44]

$$\Delta G \approx \frac{k_B T \rho_B^2(T) V_S^2}{2\sigma_{V_S}(T)} + \frac{k_B T}{2} \ln[2\pi\sigma_{V_S}(T)] \tag{9}$$

where $\sigma_{V_S} = \langle(\delta N)^2\rangle_{V_S}$ is the mean squared fluctuation in the number of molecules N in a solute-sized probe volume V_S, with $\delta N = N - \langle N\rangle_{V_S}$, and we consider the volume $V_S = 4\pi R_{HS}^3/3$ of a spherical solute of radius R_{HS} herein. These solvation free energies were then fit to $\Delta G(T) = a + bT - cT^2$, and are plotted as lines in Figure 5a,b. Solvation entropies were determined from the negative derivative of these fits, and are shown in Figure 5c,d.

The temperature dependence of hard sphere solvation is qualitatively similar in both SPC/E and GTRC water. In fact, entropy convergence is observed in the GTRC model, albeit at a convergence temperature $\tilde{T}$ approximately 100 K less than the convergence temperature in SPC/E water; $\tilde{T}_{SPC/E} = 387 \pm 8$ K and $\tilde{T}_{GTRC} = 291 \pm 7$ K, obtained from linear fitting of ΔS as a function of the heat capacity of solvation, $\Delta C_P(T) = T(\partial \Delta S/\partial T)_P$, for several temperatures.[42] Despite this quantitative distinction, the fact that the minimal reference network of GTRC water captures the phenomena of entropy convergence explicitly demonstrates that this signature of hydrophobic hydration is directly related to the energetics of the hydrogen bond network over a wide range of temperatures.

Previous work has shown that the logarithmic term in 9 has merely a secondary effect on entropy convergence, shifting $\tilde{T}$ to somewhat lower values and $\Delta S(\tilde{T})$ from zero to negative values.[40] Therefore, in order to obtain a qualitative, microscopic explanation for entropy convergence, we can neglect this term in the Gaussian approximation for the free energy, and write the solvation entropy as

$$\Delta S \approx -\left(\frac{k_B V_S^2}{2\sigma_{V_S}}\right)\rho_B^2(T)[1 - 2T\alpha_p(T)] \tag{10}$$

where $\alpha_p = -(\partial \ln \rho_B/\partial T)_P$ is the thermal expansion coefficient at constant pressure, which was determined by fitting the bulk densities to Laurent polynomials.[45] Here we have also assumed that the temperature dependence of the variance σ_{V_S} can be neglected, as has been previously established.[40] Thus within the accuracy of 10, entropy convergence is seen for $\Delta S(\tilde{T}) = 0$, and an estimate of the convergence temperature can be obtained from the intersection of $\alpha_P(T)$ and $(2T)^{-1}$. The convergence temperatures obtained for the SPC/E and GTRC models from 10 are roughly 420 and 330 K, respectively, in reasonably good agreement with the results presented above, although $\tilde{T}$ will always be overestimated in this approximation. Nonetheless, the difference between the convergence temperatures of the two models is quantitatively captured by this estimation, indicating that additional T-dependences arising in ΔG are similar in the two models, and these have been discussed in detail elsewhere.[40,42]

dx.doi.org/10.1021/jp4053067 | J. Phys. Chem. B 2013, 117, 15479−15491

In this simplified Gaussian framework, the behavior of $\alpha_P(T)$ plays a key role in entropy convergence. In the case of SPC/E water, the thermal expansion coefficient vanishes at the temperature of maximum density near 248 K.[9,45] As shown in Figure 6, $2T\alpha_P(T)$ then increases with increasing temperature but remains less than one until about 420 K, where entropy convergence is predicted to occur. The thermal expansion coefficient of GTRC water behaves in a qualitatively similar manner with $2T\alpha_P(T)$ remaining less than one until about 330 K, although $\alpha_P(T)$ is never negative, because this model lacks a density maximum near liquid−vapor coexistence.[9] The behavior of the thermal expansion coefficient is a direct consequence of the energetics of the H-bond network in both models. At ambient temperatures, the average number of hydrogen bonds per molecule approaches four in both SPC/E and GTRC water.[9] With increasing temperature, thermal fluctuations increasingly disrupt the entropically unfavorable hydrogen bond network in both models (Figure 6), which leads to an increase in the thermal expansion coefficient. However, the lower density of GTRC water permits more fluctuations as the temperature is increased, consistent with its larger compressibility and a more rapid increase in $\alpha_P(T)$, leading to a lower convergence temperature.

We also determined the temperature dependence of large solute solvation free energies following the description in the previous section. After the length scale transition, solvation is dominated by interfacial physics. As evidenced by the insets in Figure 5, hard sphere solvation free energies in this regime decrease with increasing temperature for both models, following the T-dependence of the surface tension, just as is the case for LJ solvation.

VII. LONG-RANGED INTERACTIONS AND THE SIZE DEPENDENCE OF HYDROPHOBIC ASSOCIATION

In this section, we examine the role of the various short- and long-ranged forces in the thermodynamics of hydrophobic association. In order to accomplish this task, we consider the association of pairs of spherical solutes, one pair in which both solutes are in the small-scale regime, while the other pair consists of two large solutes. We first examine the free energy as a function of solute−solute distance, R,

$$\beta W(R) = -\ln P(R) \tag{11}$$

where $P(R)$ was obtained by umbrella sampling with the harmonic biasing potential

$$U_{bias}(R) = \frac{\kappa}{2}(R - R^*)^2 \tag{12}$$

R^* is the desired value of R, and κ is a force constant tuned to achieve adequate overlap between neighboring windows. The probability distribution $P(R)$ was then constructed from the set of biased simulations using the multistate Bennet acceptance ratio method (MBAR).[27]

We first focus on hydrophobic association in the small scale regime, and consider the association of two united atom (UA) methane models, which are simply LJ particles with length and energy parameters of σ_{Me-Me} = 3.73 Å and ε_{Me-Me} = 1.234 kJ/mol, respectively.[28] Methane−water interactions were obtained from Lorentz−Berthelot mixing rules.

The potentials of mean force, $W(R)$, shown in Figure 7 for the association of two UA methanes are nearly identical for all water models under consideration. Therefore, not only does the hydrogen bond network dictate the solvation structure around individual small solutes, but also the association of solutes in this length scale regime, as expected from the results presented in the previous sections.

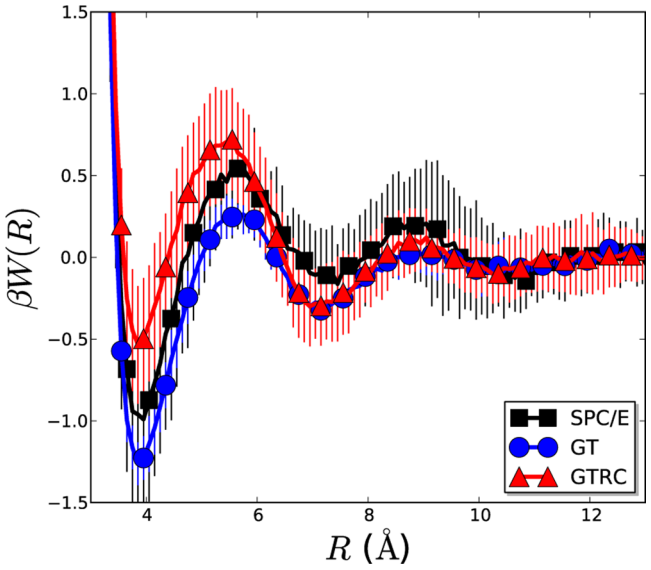

Figure 7. Potential of mean force, $W(r)$, between two UA methane particles in SPC/E, GT, and GTRC water.

We now consider the association of two large C60 fullerene molecules in the various models of water. Each C60 is represented as a single site using the coarse-graining procedure prescribed by Girifalco,[29,30] such that the fullerene−fullerene interaction is given by

$$U_{FF}(R) = -\alpha\left[\frac{1}{s(s-1)^3} + \frac{1}{s(s+1)^3} - \frac{2}{s^4}\right] + \zeta\left[\frac{1}{s(s-1)^9} + \frac{1}{s(s+1)^9} - \frac{2}{s^{10}}\right] \tag{13}$$

where α = 4.4775 kJ/mol, ζ = 0.0081 kJ/mol, $s = R/2\eta$, and η = 3.55 Å. The C_{60}−water interaction potential is

$$U_{wF}(r) = 4N\varepsilon_{wF}\frac{\sigma_{wF}^2}{r\eta}\left\{\frac{1}{20}\left[\left(\frac{\sigma_{wF}}{\eta - r}\right)^{10} - \left(\frac{\sigma_{wF}}{\eta + r}\right)^{10}\right] - \frac{1}{8}\left[\left(\frac{\sigma_{wF}}{\eta - r}\right)^{4} - \left(\frac{\sigma_{wF}}{\eta + r}\right)^{4}\right]\right\} \tag{14}$$

where N = 60, σ_{wF} = 3.19 Å, and ε_{wF} = 0.392 kJ/mol. Previous work has shown that this coarse-grained water−C_{60} interaction provides a very good representation of the solvation structure in the corresponding atomically detailed water−C_{60} system.[30]

The water−C_{60} interaction potential $U_{wF}(r)$ leads to a hydrophilic particle due to the high density of carbon sites on the surface of the C_{60} molecule. Therefore, we also consider a hydrophobic particle obtained by using only the repulsive water−C_{60} and C_{60}−C_{60} forces. This is obtained by performing a WCA-like separation of the potentials U_{FF} and U_{wF} to obtain the corresponding purely repulsive potentials $U_{0,FF}$ and $U_{0,wF}$, as detailed above for U_{sw}.

We further separate the potential of mean force as $W(R) = W_{vac}(R) + W_{solv}(R)$, where $W_{vac}(R)$ and $W_{solv}(R)$ are the vacuum and solvent-induced portions of the PMF, respectively, focusing on the latter contribution herein. The solvent-induced

dx.doi.org/10.1021/jp4053067 | J. Phys. Chem. B 2013, 117, 15479−15491

PMFs between purely repulsive C60 particles in the SPC/E and GT water models, shown in Figure 8a, are indicative of the

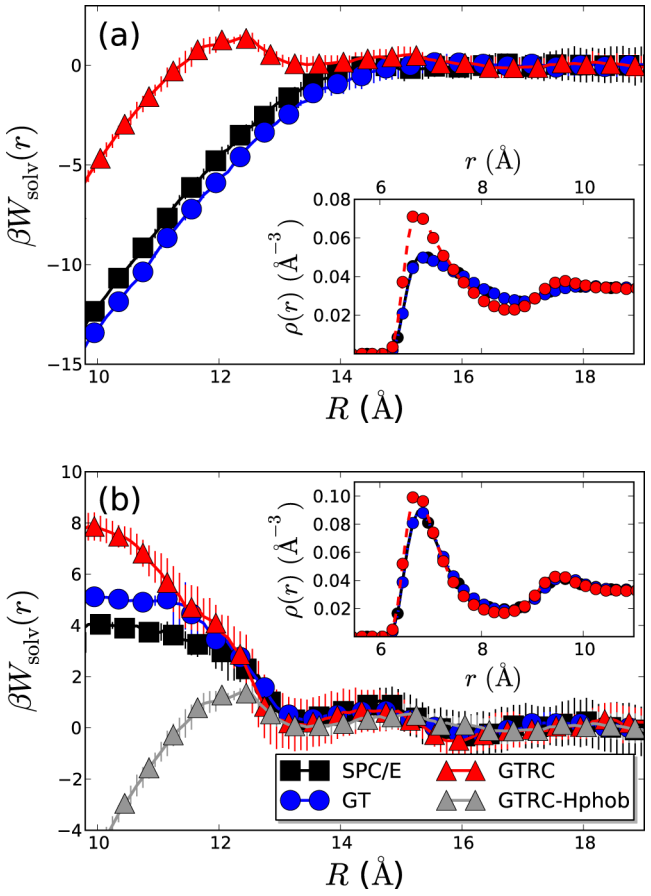

Figure 8. Solvent-induced potential of mean force, $W_{solv}(R)$, between two (a) purely repulsive and (b) attractive coarse-grained C_{60} particles in SPC/E, GT, and GTRC water. Insets in (a) and (b) show the corresponding nonuniform densities around a single coarse-grained C60 immersed in each water model. The gray curve in (b) is the GTRC PMF from panel (a).

hydrophobic effect; the association of two large apolar particles in water is barrierless, although the free energy of association is slightly lower in GT water due to its lower surface tension. Previous work has shown that the collapse of two extended hydrophobic surfaces proceeds by the formation of a vapor tube,[31,32] in which solvent molecules are evacuated from a cylindrical region between the two hydrophobes, and we will show below that the association of two repulsive fullerenes also occurs by this mechanism.

In GTRC water, however, the PMF $W_{solv}(R)$ displays a slight barrier at $R \approx 15$ Å, and another significantly higher barrier at $R \approx 12$ Å, as shown in Figure 8a. Because the $C_{60}-C_{60}$ distance does not explicitly account for changes in the behavior of the aqueous solvent, it is not a good reaction coordinate to study the association of two large hydrophobes on its own,[31,32] and $W(R)$ cannot provide an explanation for the appearance of this barrier in $W_{solv}(R)$.

To understand hydrophobic association in GT and GTRC water, we calculate the free energy as a function of the $C_{60}-C_{60}$ distance R and the density ρ_v of water in a cylindrical volume of radius 3.75 Å between the particles. This two-dimensional free energy landscape is given by $\beta W(R,\rho_v) = -\ln P(R,\rho_v)$, where $P(R,\rho_v)$ was calculated using the indirect umbrella sampling method[33] to bias the number of particles in the volume v. The harmonic potential in 12 was used to bias R. Again MBAR was used to reconstruct the probability distribution from these biased simulations.[27]

The free energy surface shown in the top panel of Figure 9 indicates that hydrophobic collapse in GT water (or SPC/E

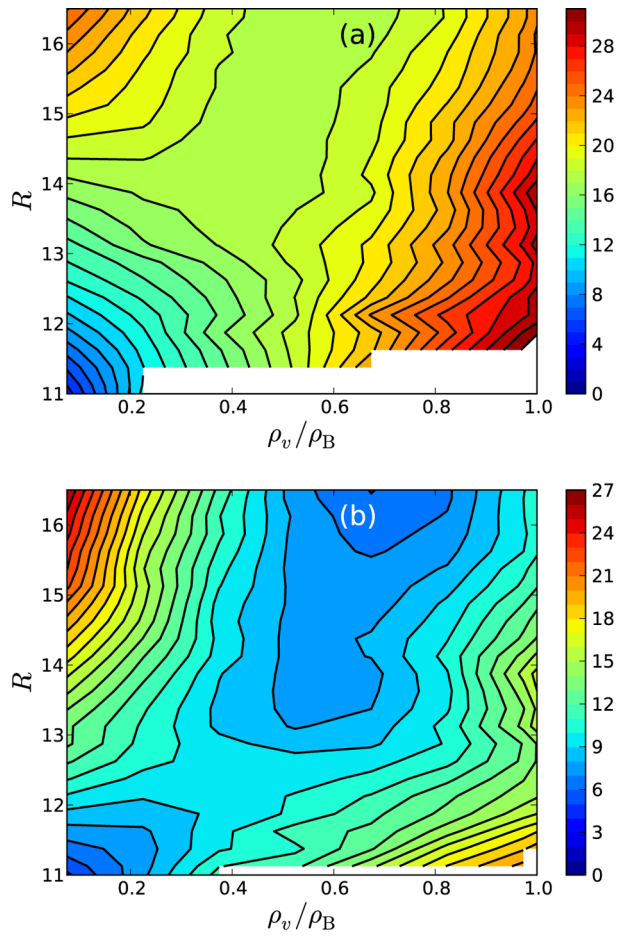

Figure 9. Free energy as a function of $C_{60}-C_{60}$ distance, R, and density of water in the observation volume v with respect to that in the bulk, ρ_v/ρ_B, for the association of two hydrophobic fullerene particles in (a) GT and (b) GTRC water models. Contour lines are spaced in increments of k_BT.

water) is indeed driven by the barrier-less formation of a vapor tube[31,32] at a $C_{60}-C_{60}$ distance between 14 and 15 Å. Hydrophobic collapse in GTRC water, on the other hand, does not follow this mechanism because capillary evaporation in the interfullerene region has been suppressed by the removal of LJ attractions in the solvent. This is consistent with the lack of drying at the interface of a single repulsive solute, as evidenced by the nonuniform densities shown in the inset of Figure 8a and would be anticipated from the results presented in Section IV.

Instead, the free energy minimum in GTRC water (for a specific value of R) remains at liquid-like densities as the $C_{60}-C_{60}$ distance is decreased, until the water molecules cannot physically remain between the fullerene particles due to repulsive core overlap near $R \approx 12$ Å. Only at this point are the solvation shell water molecules in the interfullerene region expelled. This expulsion of water molecules in the observation

dx.doi.org/10.1021/jp4053067 | J. Phys. Chem. B 2013, 117, 15479−15491

volume causes the large free energy barrier observed at the same interfullerene distance in the one-dimensional $W_{solv}(R)$ for GTRC water shown in Figure 8a.

Instead of artificially suppressing capillary evaporation between large hydrophobes by removal of solvent LJ attractions as in GTRC water, we can directly counteract the unbalanced LJ interfacial forces leading to evaporation in the GT or full water models by making the solutes sufficiently hydrophilic. LMF theory would predict very similar behavior for these two systems. This is accomplished by using the full U_{FF} and U_{wF} potentials to describe fullerene−fullerene and water−fullerene interactions, respectively. Inclusion of the water−C_{60} attractive interactions leads to an almost perfect cancellation of these unbalanced forces, as evidenced by the good agreement of the SPC/E and GT nonuniform densities with that of the GTRC model, shown in the inset of Figure 8b.

These strong solute−water attractions, arising from the high surface density of carbon atoms, render the C_{60} molecule hydrophilic, and the associated solvent-induced PMFs are repulsive for all distances. This indicates that water opposes the association of two such particles, in accord with previous results.[34] Because of the effective hydrophilicity of the particles, capillary evaporation between the particles does not occur, and $W_{solv}(R)$ is the same for all three models for $R \geq 12$ Å. At smaller separations, water is forcibly expelled from the interfullerene region due to overlap with the repulsive cores of the solutes and then differences arise due to the differing pressure of the systems.

The two-dimensional PMF $W(R,\rho_v)$ was also calculated for the case of hydrophilic fullerene particles in GT water, and is shown in Figure 10. This PMF is qualitatively very similar to

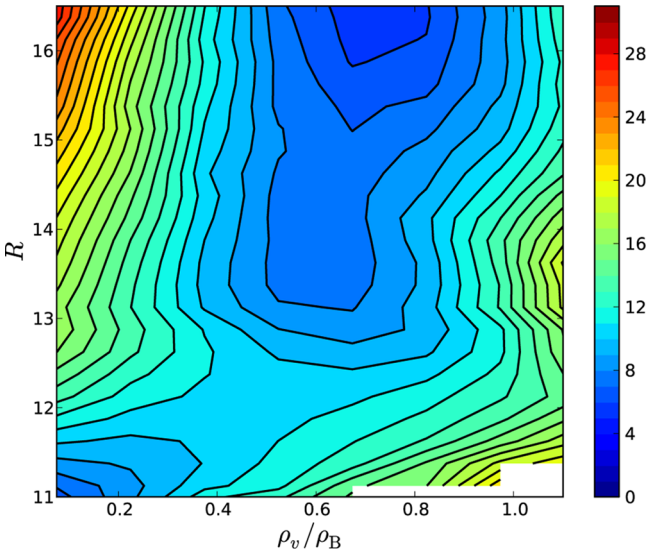

Figure 10. Free energy as a function of C_{60}−C_{60} distance, R, and density density of water in the observation volume v with respect to that in the bulk, ρ_v/ρ_B, for the association of two hydrophilic fullerene particles in GT water. Contour lines are spaced in increments of k_BT.

that shown for hydrophobic collapse in GTRC water in Figure 9b as expected. As R is decreased, the free energy minimum as a function of ρ_v remains in regions of liquid-like densities. It is not until very small R, less than 12 Å, that $W(R,\rho_v)$ develops a minimum at low ρ_v, indicating a global free energy minimum at the contact state. In fact, the solvent induced PMF $W_{solv}(R)$ between hydrophobic solutes in GTRC water is nearly identical to the PMFs obtained between hydrophilic solutes in all models until water is expelled from the interfullerene region, $R < 12$ Å, as illustrated by the curve labeled "GTRC-Hphob" in Figure 8b. In contrast to what is found for the association of large hydrophobic particles, the solvent opposes association and the contact state is stabilized by the large solute−solute attractions between hydrophilic fullerenes.

VIII. CONCLUSIONS

We have used short-ranged variants of the SPC/E water model[9] in conjunction with LMF theory to examine the crossover in the behavior of hydrophobic hydration with increasing solute size. While small scale solvation is determined exclusively by the local structure of water, i.e., the hydrogen bond network, long-ranged interactions are important for the accurate description of the hydration of large apolar solutes. Dispersion interactions lead to the phenomena of drying at extended hydrophobic interfaces, while long-ranged dipolar interactions are essential for the description of the orientational ordering of water in the vicinity of a large solute, as well as for interfacial electrostatic properties.

The truncated GT and GTRC water models also provide insight into hydrophobic interactions between solutes in the small and large length scale regimes. The local structure of water, dictated by the hydrogen bond network, is found to govern the association of two small scale solutes, a concept that has been successfully exploited to provide a theoretical framework for describing hydrophobic hydration and association at small length scales.[44] Moreover, previous work has shown that coarse-grained models, whereby water molecules interact via a single spherically symmetric pairwise potential, can reproduce the thermodynamics of association of two methanes.[46,47] From the results presented here, it is not surprising that such coarse-grained models can capture features of small scale hydrophobicity, since these models also describe the bulk structure of water with near quantitative accuracy.

The association of two large scale hydrophobes involves the formation of an intersolute vapor tube, and the unbalanced forces arising from water−water LJ attractions are found to be of the utmost importance for this mechanism of hydrophobic association. In this regime the coarse-grained water models will fail completely. Cancellation of the effects of interfacial unbalanced forces, either by explicit removal of solvent−solvent LJ attractions (as in GTRC water) or by addition of large solute-water attractions that counterbalance these forces, suppresses capillary evaporation between two large solutes. As a result the solute surface is wet by the aqueous solvent, and free energy barriers to the association of two large hydrophilic solutes exist. In all these cases comparison of results in the full model with those from the short-ranged GT and GTRC water models provides a simple and physically suggestive way to disentangle the effects of longer-ranged dispersive and Coulomb interactions from properties of the local hydrogen bond network.

AUTHOR INFORMATION

Corresponding Authors

*E-mail: rremsing@umd.edu.
*E-mail: jdw@umd.edu.

Notes

The authors declare no competing financial interest.

■ ACKNOWLEDGMENTS

This work was supported by the National Science Foundation (Grant CHE0848574). We are grateful to Shekhar Garde, Hari Acharya, David Chandler, and Jocelyn Rodgers for many helpful discussions.

■ REFERENCES

(1) Ball, P. Water as an active constituent in cell biology. *Chem. Rev.* **2008**, *108*, 74−108.
(2) Chandler, D. Interfaces and the driving force of hydrophobic assembly. *Nature* **2005**, *437*, 640−647.
(3) Berne, B. J.; Weeks, J. D.; Zhou, R. Dewetting and hydrophobic interaction in physical and biological systems. *Annu. Rev. Phys. Chem.* **2009**, *60*, 85−103.
(4) Stillinger, F. H. Structure in aqueous solutions of nonpolar solutes from the standpoint of scaled-particle theory. *J. Solution Chem.* **1973**, *2*, 141−158.
(5) Lum, K.; Chandler, D.; Weeks, J. D. Hydrophobicity at small and large length scales. *J. Phys. Chem. B* **1999**, *103*, 4570−4577.
(6) Weeks, J. D. Connecting local structure to interface formation: A molecular scale van der Waals theory of nonuniform liquids. *Annu. Rev. Phys. Chem.* **2002**, *53*, 533−562.
(7) Huang, D. M.; Chandler, D. Cavity formation and the drying transition in the Lennard-Jones fluid. *Phys. Rev. E* **2000**, *61*, 1501−1506.
(8) Huang, D. M.; Geissler, P. L.; Chandler, D. Scaling of hydrophobic solvation free energies. *J. Phys. Chem. B* **2001**, *105*, 6704−6709.
(9) Remsing, R. C.; Rodgers, J. M.; Weeks, J. D. Deconstructing classical water models at interfaces and in bulk. *J. Stat. Phys.* **2011**, *145*, 313−334.
(10) For a different molecular based truncation scheme, see Nezbeda, I. Towards a unified view of fluids. *Mol. Phys.* **2005**, *103*, 59−76. and Nezbeda, I.; Jirsak, J. Water and aqueous solutions: Simple non-speculative model approach. *Phys. Chem. Chem. Phys.* **2011**, *13*, 19689−19703. While such short-ranged models can give reasonably accurate radial distribution functions, their description of dipole angle correlation functions in acetonitrile and water is much less accurate than that given by the site based Gaussian truncated models discussed herein, for reasons explained in Rodgers, J. M.; Hu, Z.; Weeks, J. D. On the efficient and accurate short-ranged simulations of uniform polar molecular liquids. *Mol. Phys.* **2011**, *109*, 1195−1211.
(11) Weeks, J. D.; Chandler, D.; Andersen, H. C. Role of repulsive forces in determining the equilibrium structure of simple liquids. *J. Chem. Phys.* **1971**, *54*, 5237−5247.
(12) Widom, B. Intermolecular forces and the nature of the liquid state. *Science* **1967**, *157*, 375−382.
(13) Rodgers, J. M.; Weeks, J. D. Local molecular field theory for the treatment of electrostatics. *J. Phys.: Condens. Matter* **2008**, *20*, 494206.
(14) Berendsen, H. J. C.; Grigera, J. R.; Straatsma, T. P. The missing term in effective pair potentials. *J. Phys. Chem.* **1987**, *91*, 6269−6271.
(15) Rodgers, J. M.; Weeks, J. D. Interplay of local hydrogen-bonding and long-ranged dipolar forces in simulations of confined water. *Proc. Natl. Acad. Sci. U.S.A.* **2008**, *105*, 19136.
(16) Rodgers, J. M.; Weeks, J. D. Accurate thermodynamics for short-ranged truncations of Coulomb interactions in site−site molecular models. *J. Chem. Phys.* **2009**, *131*, 244108.
(17) Smith, W.; Yong, C.; Rodger, P. DL_POLY: Application to molecular simulaton. *Mol. Simul.* **2002**, *28*, 385−471.
(18) Berendsen, H. J. C.; Postma, J. P. M.; van Gunsteren, W. F.; DiNiola, A.; Haak, J. R. Molecular dynamics with coupling to an external bath. *J. Chem. Phys.* **1984**, *81*, 3684.
(19) Allen, M. P., Tildesley, D. J.: Computer Simulation of Liquids; Oxford: New York, 1987.
(20) Acharya, H., Garde, S. Rensselaer Polytechnic Institute, Troy, NY. To be submitted for publication.
(21) Huang, D. M.; Chandler, D. The hydrophobic effect and the influence of solute-solvent attractions. *J. Phys. Chem. B* **2002**, *106*, 2047−2053.
(22) Andersen, H. C.; Weeks, J. D.; Chandler, D. Relationship between the hard-sphere fluid and fluids with realistic repulsive forces. *Phys. Rev. A* **1971**, *4*, 1597−1607.
(23) Stillinger, F. H.; Ben-Naim, A. Liquid−vapor interface potential for water. *J. Chem. Phys.* **1967**, *47*, 4431−4437.
(24) Luzar, A.; Chandler, D. Effect of environment on hydrogen bond dynamics in liquid water. *Phys. Rev. Lett.* **1996**, *76*, 928−931.
(25) Bennett, C. H. Efficient estimation of free energy differences from Monte Carlo data. *J. Comput. Phys.* **1976**, *22*, 245−268.
(26) Pohorille, A.; Jarzynski, C.; Chipot, C. Good practices in free-energy calculations. *J. Phys. Chem. B* **2010**, *114*, 10235−10253.
(27) Shirts, M. R.; Chodera, J. D. Statistically optimal analysis of samples from multiple equilibrium states. *J. Chem. Phys.* **2008**, *129*, 124105.
(28) Cornell, W. D.; Cieplak, P.; Bayly, C. I.; Gould, I. R.; Merz, K. M.; Ferguson, D. M.; Spellmeyer, D. C.; Fox, T.; Caldwell, J. W.; Kollman, P. A. A second generation force field for the simulation of proteins, nucleic acids, and organic molecules. *J. Am. Chem. Soc.* **1995**, *117*, 5179−5197.
(29) Girifalco, L. A. Molecular properties of C_{60} in the gas and solid phases. *J. Phys. Chem.* **1992**, *96*, 858−861.
(30) Choudhury, N. A molecular dynamics simulation study of buckyballs in water: Atomistic versus coarse-grained models of C_{60}. *J. Chem. Phys.* **2006**, *125*, 034502.
(31) Lum, K.; Luzar, A. Pathway to surface-induced phase transition of a confined fluid. *Phys. Rev. E* **1997**, *56*, R6283.
(32) Willard, A. P.; Chandler, D. The role of solvent fluctuations in hydrophobic assembly. *J. Phys. Chem. B* **2008**, *112*, 6187−6192.
(33) Patel, A. J.; Varilly, P.; Chandler, D.; Garde, S. Quantifying density fluctuations in volumes of all shapes and sizes using indirect umbrella sampling. *J. Stat. Phys.* **2011**, *145*, 265−275.
(34) Li, L.; Bedrov, D.; Smith, G. D. A molecular-dynamics simulation study of solvent-induced repulsion between C_{60} fullerenes in water. *J. Chem. Phys.* **2005**, *123*, 204504.
(35) Varilly, P.; Patel, A. J.; Chandler, D. An improved coarse-grained model of solvation and the hydrophobic effect. *J. Chem. Phys.* **2011**, *134*, 074109.
(36) ten Wolde, P. R.; Chandler, D. Drying-induced hydrophobic polymer collapse. *Proc. Natl. Acad. Sci. U.S.A.* **2002**, *99*, 6539−6543.
(37) Egelstaff, P. A.; Widom, B. Liquid surface tension near the triple point. *J. Chem. Phys.* **1970**, *53*, 2667.
(38) Rajamani, S.; Truskett, T. M.; Garde, S. Hydrophobic hydration from small to large lengthscales: Understanding and manipulating the crossover. *Proc. Natl. Acad. Sci. U.S.A.* **2005**, *102*, 9475−9480.
(39) Sedlmeier, F.; Netz, R. R. The spontaneous curvature of the water−hydrophobe interface. *J. Chem. Phys.* **2012**, *137*, 135102.
(40) Garde, S.; Hummer, G.; García, A. E.; Paulaitis, M. E.; Pratt, L. R. Origin of entropy convergence in hydrophobic hydration and protein folding. *Phys. Rev. Lett.* **1996**, *77*, 4966−4968.
(41) Hummer, G.; Garde, S.; García, A. E.; Paulaitis, M. E.; Pratt, L. R. Hydrophobic effects on a molecular scale. *J. Phys. Chem. B* **1998**, *102*, 10469−10482.
(42) Sedlmeier, F.; Horinek, D.; Netz, R. R. Entropy and enthalpy convergence of hydrophobic solvation beyond the hard-sphere limit. *J. Chem. Phys.* **2011**, *134*, 055105.
(43) Gaziano, G. A van der Waals approach to the entropy convergence phenomenon. *Phys. Chem. Chem. Phys.* **2004**, *6*, 406−410.
(44) Hummer, G.; Garde, S.; Garc′ia, A. E.; Pohorille, A.; Pratt, L. R. An information theory model of hydrophobic interactions. *Proc. Natl. Acad. Sci. U.S.A.* **1996**, *93*, 8951−8955.
(45) Ashbaugh, H. S.; Collett, N. J.; Hatch, H. W.; Staton, J. A. Assessing the thermodynamic signatures of hydrophobic hydration for several common water models. *J. Chem. Phys.* **2010**, *132*, 124504.
(46) Chaimovich, A.; Shell, M. S. Anomalous waterlike behavior in spherically-symmetric water models optimized with the relative entropy. *Phys. Chem. Chem. Phys.* **2009**, *11*, 1901−1915.

(47) Hammer, M. U.; Anderson, T. H.; Chaimovich, A.; Shell, M. S.; Israelachvili, J. The search for the hydrophobic force law. *Faraday Discuss.* **2010**, *146*, 299−308.